

Studies of the Human Breathing

Roman Neronov
Modern Medical Technology
Medical Holding
Saint-Petersburg, Russia
nrvspb@mail.ru

Gennadiy Lukyanov, Anna Rassadina,
Aleksey Voronin, Aleksey Malyshev
ITMO University
Saint-Petersburg, Russia
gen-lukjanow@yandex.ru,
a.a.rassadina@gmail.com

Thomas Seeger
University of Siegen
Siegen, Germany
thomas.seeger@uni-
siegen.de

Abstract—The article presents four branches of multi-year research of human breathing. They are (1) modeling and study the movement of the convective flows in the artificial models of nose; (2) numerical modeling of the convective flows movement on the computer models; (3) breathing research with the help of diagnostic equipment; (4) determination of the exhaled air composition. In all our studies the breathing was examined as a dynamical process. The results of pressure, temperature, velocity and concentration CO_2 measuring in the nostrils and in the significant parts of the artificial model of nasal cavity are presented. For this measurements estimated the correlation entropy, correlation dimension. The 3D geometrical model of human nasal cavities obtained from computer-aided tomography data using Mercury Amira program is also given. The 3D unstructured mesh with $1,5 \times 10^7$ finite elements was constructed after the segmentation using Altair Hypermesh software had been finished. The mesh was used to set up an unsteady simulation of airflow inside the obtained geometrical model. Application of DES method on the mesh of a good quality made it possible to distinguish the small-scale turbulent swirls inside the flow. A gas sensor based on spontaneous Raman scattering is proposed for the compositional analysis of single breath events. The Raman sensor is able to detect all the major gas components, i.e. N_2 , O_2 , CO_2 , and H_2O at ambient pressure with a high temporal resolution. Concentration fluctuations within a single breath event could be resolved.

I. INTRODUCTION

The human upper airway, including the nasal cavity and paranasal sinuses, is a complex geometric shape of irregular cross-section, with numerous protuberances, undulations, derivations. The nose dysmorphology leads to difficulty of breathing. The long dysmorphology of nasal breathing virulent of lack of oxygen supply to lungs; leads to disruption of the brain hemodynamic (headache, rapid fatigability, amnesia), to nervous system disorder and to bronchial allergy. The children suffer from an epilepsy spells, night incontinence of urine.

For the foregoing reasons, the studies of the internal nose morphology to the movement of air flow during breathing are relevant. Identify of influence pattern of the air exchange processes between the nasal cavity and paranasal sinuses studies are relevant as well. Studies will be ministerial to the development of fundamental region of knowledge (it will correct physiology knowledge regarding the air flow movement inside the nasal cavity at breathing) both and

applied research (early diagnostic of respiratory diseases methods creation).

Measurements of the convective flow parameters inside the nasal cavity are scarcely impossible because of its complicated, irregular structure and miniaturization of its size. Deep knowledge will be received from the complex studies, including the numerical modeling of the convective flows movement on the computer models; modeling the movement of the convective flows in the artificial models of nose; breathing research with the help of diagnostic equipment. With the implementation of these studies we create method of early respiratory and other human organs diseases diagnostic.

Specific line of research is the studies of expired air compositional analysis methods. Molecular composition of expired air includes more than 600 volatile and nonvolatile compounds [1]. The composition and concentration of exhaled molecules are determined by the processes of natural chemical transformation of air and food molecules coming from the environment into the internal organs. They, as well as blood and other biological waste products, provide information about the functional state of the organism. It was found that about 20 of the most sensitive to changes in the functional state of the body's molecules of exhaled air can be used as natural biomarkers (diagnosis objects) of a various diseases.

Within our investigation, the composition of the exhaled air was evaluated using the Raman spectroscopy.

Specific character of the execute study is what the human respiration was view as a dynamic processes. For the first time the dynamic changes of the breath parameters rather than the average values of its parameters was analyzed.

The term “dynamic” is often interpreted not in terms of the passing of the test process, but as, for example, of the possibilities of the sensors used in the measurements.

In all directions we analyze the parameters of dynamical fluctuations. It was attractor reconstruction from time series data, calculation of power spectral density through the discrete Fourier transform, calculation of correlation dimension and the correlation entropy.

This information can be used to refine existing models of the processes and, in turn, allows better understand the evolution of the processes, allows to receive more accurate assessment of the human condition.

II. METHOD AND DEVICES

A. Numerical modeling of respiration

1) The mathematical description of the model of the detached eddies

Numerical simulations of fluid and gas turbulent flows is a very complex and at the same time a crucial task, arising from various fields of science and technology. Application of mathematical turbulent models at practice has been developed as a solution of essential more complicated problems. The high-velocity air simulations at aerospace applications, the atmospheric circulation eddies parameters determination and others are among them.

The first mathematical model was proposed by L. Prandtl in 1925. The model allowed performing a viscous fluid substances motion calculation through the averaged Navier-Stokes equations and mixing length parameter. Since then various researchers all over the world have proposed many models of turbulence for various engineering applications. Such as the algebraic models, the Reynolds Averaged Navier-Stokes (RANS) with one or two differential equations to determine the eddy viscosity, Reynolds Stress Modeling (RSM), and also more sophisticated Large Eddy Simulation (LES) models and others. Although RANS and LES models development was completed almost simultaneously, currently the LES models application is difficult because of lack of sufficient computing power.

Proposed by P. Spalart [2] in 1997 Detached Eddy Simulation (DES) method is a compromise between the two RANS and LES models. DES method is a solution of three-dimensional nonstationary equations with a single model of turbulence. The single turbulence model used as subgrid-scale model with high grid resolution, and as Unsteady RANS (URANS) in areas, where the grid resolution is insufficient [3]. The basic concept of the DES method is to use the LES model for zones of free flow and to use RANS model near boundary-layers and as subgrid functions. This prevents excessive fragmentation of the computational mesh at near-wall region. Thus, we achieve a sufficiently accurate solution of nonstationary hydrodynamic problem with acceptable level of required computer efficiency.

Note that the original representation of the P. Spalart one-parameter model was used as RANS model. This model is known as a Spalart-Allmaras (SA) model. In more recent papers [3],[4] two-parameter RANS model (SST (Menter's Shear Stress Transport turbulence model) was assumed [5].

The following steps were upgraded versions of this model – Delayed Detached Eddy Simulation (DES – DDES) [6] and Improved Delayed Detached Eddy Simulation (IDDES) [7]. These models are suitable for a wide range of unseparated flow problems. The methods can be applied to transient turbulent flows modeling.

In this study the turbulent flows simulation for irregular-shaped areas by the DES-SST method was carried out. Nasal cavities and paranasal sinuses were studied as irregular-shaped areas.

In order to describe a fluid flow the Navier-Stokes equations are used. The equation system includes continuity equation and equations for the flow velocity.

The continuity equation is:

$$\frac{\partial \rho}{\partial \tau} + \frac{\partial \rho u_j}{\partial x_j} = 0 \tag{1}$$

The motion equation is:

$$\frac{\partial \rho u_j}{\partial \tau} + \frac{\partial \rho u_j u_i}{\partial x_j} = \frac{\partial P}{\partial x_i} + \frac{\partial \tau_{ij}}{\partial x_j} \tag{2}$$

where, u_i, u_j are the flow velocity component, ρ is the density, τ_{ij} is the deviatoric stress tensor.

The most significant advantage of DES algorithm over RANS method is based on possibility to gather the information on high frequency eddies inside the flow which is gained by replacing of time filtration (RANS models) with the spatial filtration (DES methods).

The mathematical formulation of velocity field vector filtration $u(x, t)$ is:

$$\bar{u}(x, t) = \int G(r, x) u(x - r, t) dr \tag{3}$$

where $G(r, x)$ - filtration function. The width of the filter determining the function $G(r, x)$ can be determined explicitly, or with the size of the finite element mesh. Equations (1) and (2) filtered according to the equation (3) can be simplified to this form:

$$\begin{aligned} \frac{\partial \rho \bar{u}_i}{\partial \tau} + \frac{\partial \rho \bar{u}_i \bar{u}_j}{\partial x_j} = & - \frac{\partial}{\partial x_i} \left(\bar{p} + \frac{2}{3} \mu \frac{\partial \bar{u}_k}{\partial x_k} \right) + \\ & + \frac{\partial}{\partial x_i} \left(\mu \left(\frac{\partial \bar{u}_i}{\partial x_j} + \frac{\partial \bar{u}_j}{\partial x_i} \right) \right) - \rho \tau_{ij}^r \end{aligned} \tag{4}$$

where $\tau_{ij}^r = \bar{u}_j \bar{u}_i - \bar{u}_j \bar{u}_i$ is the deviatoric stress tensor. This parameter has to be determined in order to solve the equations (4).

Simulation of the stress deviator tensor is performed by so-called eddy-viscosity subgrid -scale models, such as the Smagorinsky model. This model contains the hypothesis of proportionality of the stress deviator tensor to strain velocity tensor of filtered area and is structurally similar to the Boussinesq hypothesis.

In accordance to DES method the linear scale l_{RANS} is replaced with the following ratio:

$$l_{DES} = \min \{ l_{RANS}, C_{DES}, \Delta \}, \quad (5)$$

where, l_{DES} – DES linear scale, C_{DES} – constant, Δ – a filter size, is determined as:

$$\Delta = \max \{ \Delta_x, \Delta_y, \Delta_z \}, \quad (6)$$

where, $\Delta_x, \Delta_y, \Delta_z$ is the finite element size.

The replacement result is congruence $l_{DES} = l_{RANS}$ and the DES model performs functions as a RANS model if the size of filter (computational mesh) is too crude and $C_{DES}\Delta > l_{RANS}$.

Otherwise, the DES model is transformed into LES model and complies with solution of filtered equations (4). Thus, DES method allows to reach significantly transient solution of the question problem.

2) *The geometrical model of internal nasal channels*

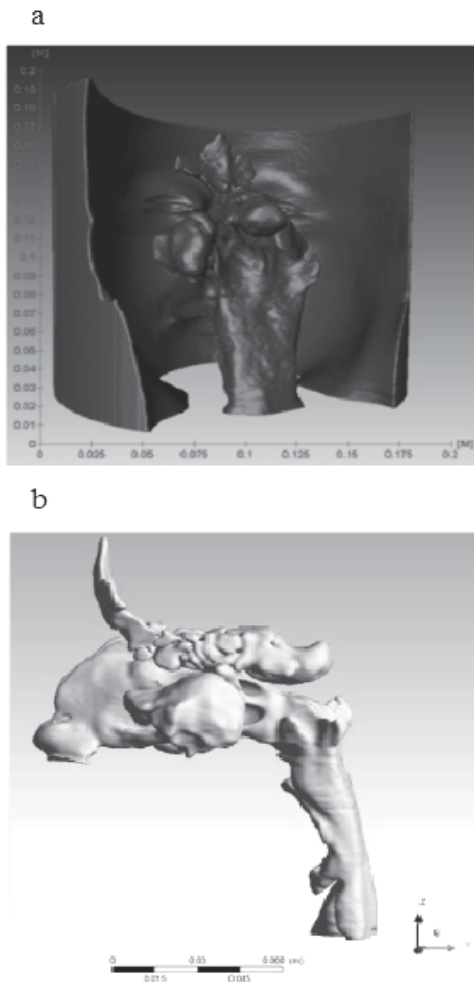


Fig. 1. The geometric model reconstructed according to the data of patients' computer tomography: (a) base model; (b) edit model

The geometrical model of human internal nasal channels was reconstructed from the computed tomography (CT) scans of patients of “Modern medical technology” medical holding (St. Petersburg) with the help of specialized Mercury Amira software package. The three-dimensional geometric model representation is shown in Fig. 1.

The model segmentation from the Fig. 1 to the “entrance”, “exit”, “wall” boundaries was carried out with the help of Altair Hypermesh software package. Construction of the finite elements volume mesh was made with the help of Ansys Icem CFD software package.

B. *Artificial models of nose*

The experimental investigations of human respiration have a more long history. The first solid models have been produced in 20-s and 30-s of the previous century (authors Mink P.(1920), Hofbauer (1921), Takahashi K. (1923), Businger O. (1936), Scheideler J. (1938)) [8],[9]. These investigations remain actual still. The fact is the complicated fine structure of nasal cavities vastly impedes the investigations of convective flows, even with solid models. As a rule – these are only visual observations of stained liquid or smoke moving in the solid model. And the model could be sized for the convenient observation.

The works [10], [11] use natural-sized solid models including left and right nose halves with cavities and nasal septum. Air was used as a medium. Observation of changes in convective flow in several important model areas was performed with measuring of the flow parameters (pressure, velocity) with the miniature sensors. These experimental investigations show the exclusive importance of the measurements of high-frequency increments in pulsations of dynamic parameters of turbulent airflow in the nasal channels, in the applications of diagnostics of upper airways deceases.

The artificial solid model of the nasal cavity was created on the basis of the computer tomography data (Fig. 1 a, b). The model was used for an experimental simulation of breathing process (Fig. 2 a, b). The air motion imitation of breathing was performed through a tube that was fixed to the nasopharynx area of the model. The piezoresistive pressure sensors through thin shunt tubes have been connected with multiple places of the solid model for the pressure drop fixing of air flow in time. They are:

- the left and the right entrances of nose (vestibule of nose);
- the left and the right maximally sinuses;
- the left and the right parts near nasal septum (aria of ridge of nose);
- the left and the right frontal sinuses;
- the left and the right anterior, middle and posterior ethmoid cells;
- the left and the right sphenoid cells;
- choanae.

Signals received from pressure sensors supplied to the data automation subsystem, which control and synchronize the sensors. Settings and data recording performed by software provided by the manufacturer.

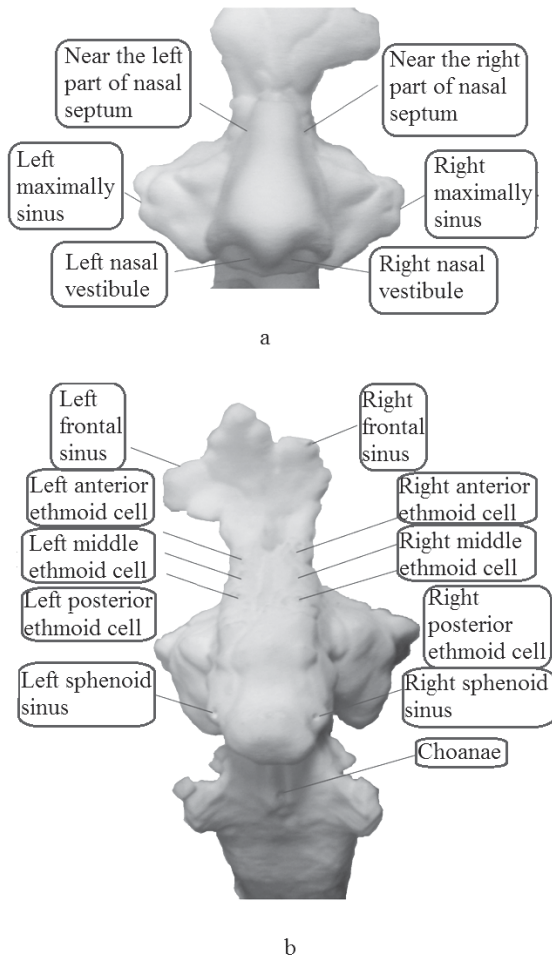


Fig. 2. The places of location thin shunt tubes for measuring of pressure at the artificial solid model of human nose cavity: (a) front view of artificial model; (b) back view

Data processing was performed at Matlab mathematical modeling package. For data processing was written the software application which allow to convert voltage output value of the sensors in pascal (Pa), filter data, delete steady component at the pressure transducer readings, which the sensors produces as a default, display depending on the time domain.

C. Sensor devices

At the present time widely accepted the anterior rhinomanometry and acoustic rhinometry methods of diagnosis of respiratory diseases. The diagnosable parameter of the anterior rhinomanometry method is the nose resistance, identifying as $R=\Delta p/\omega$, where Δp – pressure drop, ω - flow rate. Pressure and flow sensors are placing in the diagnostic tube, connected to the breathing organs (nose or mouth). It is noninvasive measurements and portable apparatus, but important diagnostic data are loss in tube and natural breathing are distortion. With this end in view the sound with frequency

150-10000 Hz is sent to the nasal cavity where reflected from hindrance and back into the microphone (echo-sounder principle)

The method is used only as aid in the diagnosis to the method of the anterior rhinomanometry.

We designed some models of sensor for the dynamic measurements of the breath parameters in vestibule of nose (nostrils) without any tube for sensor elements (Fig. 3).

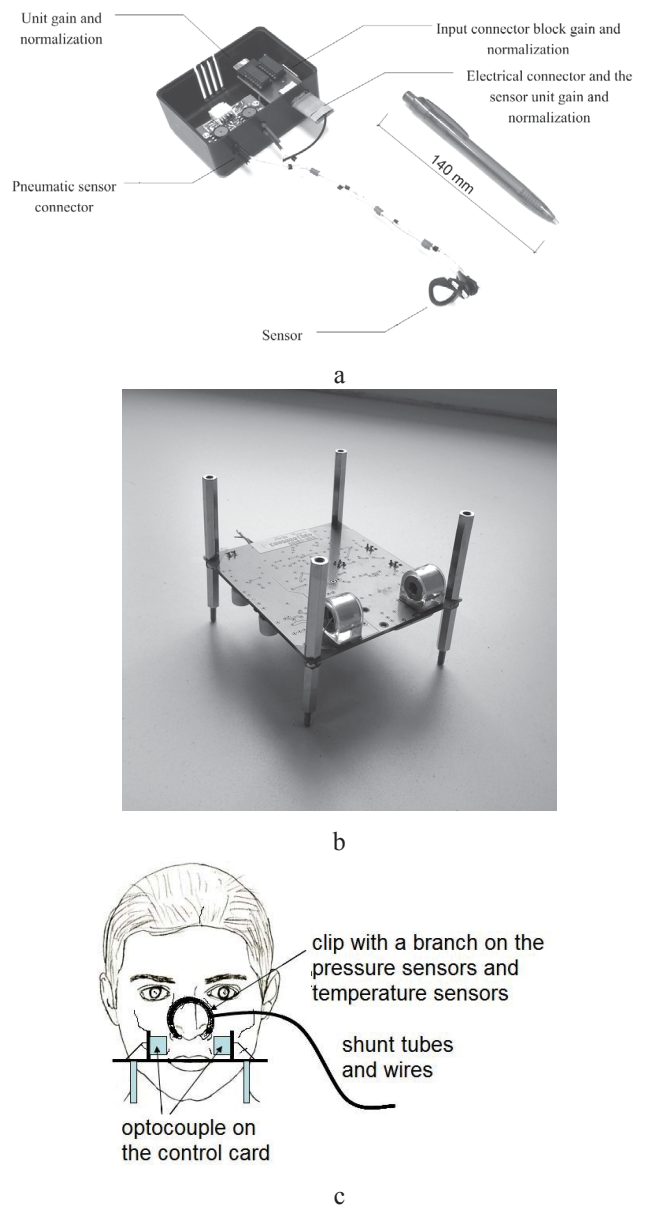


Fig. 3. Sensing device based on the pressure sensors (a), IR optocouple (b) and the experimental scheme used (c).

The sensor [12] is designed for measuring rapid fluctuations of temperature, pressure and velocity of air flow at the vestibule of nose (in nostrils). Now we use the sensor now with slight modifications. The basic requirements for the created sensor were – to receive the lowest possible distortion of air flow and to have response to extremely fast changes in temperature, pressure and velocity. The device has two

miniaturized and highly sensitive temperature sensor and two miniaturized and highly sensitive pressure sensor. The air flow velocity is not measured at present time. Previous studies have shown that the curves of fluctuations of temperature, pressure and air velocity repeat each other, therefore, it is not required to measure directly all the parameters to perform diagnostics. In principle, one parameter is enough for the diagnosis. Thermocouple wires (diameter of 0.08 mm) and a shunt tubes to pressure sensors (0.5 mm diameter) placed on the diagnostic clip sensor device (Fig. 3a). The signals of the sensors are supplied to the amplifier and then to the multi-channel device data acquisition National Instruments.

The basis of diagnosis is methods of nonlinear dynamics:

- calculation correlation sum, $C(\varepsilon)$, correlation dimension, D_2 , and the correlation entropy, K_2 :

$$C(\varepsilon) = \lim_{m \rightarrow \infty} \frac{1}{m^2} \sum_{\substack{i, j=1 \\ i \neq j}}^m H\left(\varepsilon - \|x_i - x_j\|\right) \quad (7)$$

$$H = \begin{cases} 1, & \left(\varepsilon - \|x_i - x_j\|\right) \geq 0 \\ 0, & \left(\varepsilon - \|x_i - x_j\|\right) < 0 \end{cases} \quad (8)$$

$$D_2 = \lim_{\varepsilon \rightarrow \infty} \frac{\log C(\varepsilon)}{\log \varepsilon} \quad (9)$$

$$K_2 = \lim_{\tau \rightarrow 0} \lim_{\varepsilon \rightarrow 0} \lim_{ED \rightarrow \infty} \frac{1}{\tau} \cdot \log \left(\sum_{i_1 \dots i_N} \frac{C_{ED}(\varepsilon)}{C_{ED+1}(\varepsilon)} \right) \quad (10)$$

where, H - Heaviside step function, ε - diameter of volume elements covered an attractor, x_i, x_j - points in some metric space with distances $\|x_i - x_j\|$ between any pair of points, $C_{ED}(\varepsilon)$ - correlation integral of embedding dimension;

- calculation of power spectral density through the discrete Fourier transform;
- attractor reconstruction from time series data.

A dynamic fluctuation of air flow inevitable leads to the formation of eddies. These eddies are rotate. We suppose that during the rotation, the air composition concentrations cannot be constant and probably they change like pressure, temperature and other parameters of breathing. As a result the latest model has been designed on the basis of the sensor measuring fluctuations of carbon dioxide (CO_2), which showed good compatibility with our other experimental data.

The possibilities of using a LED-photodiode optocouple ("LED Microsensor NT", Ltd.) as a sensor device for contactless measurements of the dynamic fluctuations of CO_2 concentration in the human breath was investigated in this study (Fig. 3b).

To test the sensitivity of the method, the measurements of CO_2 concentration oscillations during the breathing were performed synchronically with measurements of pressure oscillations. The experimental scheme of synchronous measurements is presented in Fig. 3c. Clip with pressure and temperature sensors tap was attached to the nasal septum. The board has been placed near patient's nose, at a distance of ~5 cm. The signal from the pressure sensors and the optocouple was analyzed with the LeCroy WaveSurfer 3000 oscilloscope.

D. Raman sensor system for an online analysis of human inhalation and exhalation

In recent years there was a steady tendency to focus e studies of the Human Respiration on the gas composition of expired air [13],[14],[15]. Therefore, it is more and more important to develop new methods and technologies which could open the potential for creation of an online sensor system that would allow precise measurement of the gas composition of the exhaled air. In this case also a fast data acquisition of all gas compound within a time resolution of 200 ms to 500 ms is necessary in order to clearly resolve the dynamic behavior of each breath event. This requirement can be met with use of spectroscopic techniques like infrared absorption techniques [16]. Nevertheless a fast analysis of a multicomponent gas mixture by such absorption based techniques requires in most cases a specific detector system for each component. Spontaneous Raman scattering provides an interesting alternative detection method for identification and determination of all relevant compounds in the breathing gas during consecutive breath events [17],[18]. In principle, it allows the simultaneous detection of any polyatomic compounds with high temporal resolution using only one sensor system. Due to the high content of information, spontaneous Raman scattering belongs to the mostly developed spectroscopic techniques. In spite of being a challenging technique due to a weak signal, the linear Raman spectroscopy seems to be perfectly suited for the application in gas sensor monitoring [17]. Additionally there is no need for a sample preparation, which enables an access to in situ measurements. The sensor presented in this paper requires no sample preparation and can detect all the main air components such as O_2 , CO_2 , N_2 and H_2O , at a pressure between 949 hPa and 1004 hPa within a short measurement time. Development of the sensor hardware and especially the signal enhancement by using a multi-pass approach is explained. Also the calibration procedure with use of the H_2O vapor is described. Finally, its successful application is demonstrated during consecutive human breath events.

The well known principles of spontaneous Raman scattering can be found in literature (see e.g. [19],[20]). Therefore only a brief summary is presented here. The spontaneous Raman scattering is a result of an inelastic interaction between light and matter. That means that the scattered radiation frequency is shifted in respect to the incident laser radiation frequency. The respectively red- and blue-shifted signals are defined as the Stokes and anti-Stokes Raman scattering. The observed frequency shift value depends on the energy difference between the virtual energy levels of the involved molecules:

$$\Delta v_R = T'(v', J') - T''(v'', J'') \quad (11)$$

The parameters marked with one prime are related to the upper energy level and the parameters marked with two primes are related to the lower energy state. The energy term $T(v, J)$ include the values of the vibration and the rotation energies of the molecule, it can be determined in dependence on the vibrational quantum number v and the rotational quantum number J . In the simple case of diatomic molecule, for instance N_2 , the energy term can be expressed by:

$$\begin{aligned} T(v, J) = & \omega_e \left(v + \frac{1}{2} \right) - \omega_e x_e \left(v + \frac{1}{2} \right)^2 + \dots \\ & + \left[B_e - \alpha_e \left(v + \frac{1}{2} \right) + \dots \right] J(J+1) - \quad (12) \\ & - \left[D_e + \beta_e \left(v + \frac{1}{2} \right) + \dots \right] J^2 (J+1)^2 + \dots \end{aligned}$$

Here, ω_e , $\omega_e x_e$, B_e , α_e , D_e , β_e are the molecule specific constants which can be found in compilation data books, e.g., G. Herzberg [21],[22] for diatomic and polyatomic molecules. One can see from eq. (7) that the energy is influenced only by the molecule specific constants. Consequently, also the Raman shift Δv_R is a molecule specific parameter that can be used as a fingerprint of this particular molecule. This fingerprint can be used either for the compound identification or for a quantitative analysis of the gas samples while measuring the signal intensity. The detected intensity I_i of a vibrational Stokes Raman line of the compound i can be written as

$$I_i = k \Omega \frac{\partial \sigma}{\partial \Omega} n_i l I_0 \quad (13)$$

where Ω is the collecting solid angle of the optics, $\partial \sigma / \partial \Omega$ is the differential Raman scattering cross section by the compound, l is the length of the measurement volume, and I_0 is the incident laser intensity. The factor k depends on the experimental setup, and n_i is the parameter of interest, i.e. the number density of the specific gaseous compound i inside the probe volume. The spectrum of a gas mixture is in principal a superposition of the spectra of the pure substances

within the mixture. By evaluating the intensity of the individual Raman spectral bands, the compound concentration can be easily determined. In case of the overlapping bands, a contour fit algorithm can be applied to reconstruct the individual compound signal.

III. RESULTS

A. Results of numerical modeling of respiration

The results of transient numerical simulations of nonstationary air flow (velocity field) in internal nasal channels (Fig. 1) are presented in a Fig. 4. The simulation was performed using the DES-SST method based on the volume irregular mesh of $1,5 \times 10^7$ tetrahedral structure forming elements.

The following boundary conditions were assumed:

The pressure in the vestibule of nose (“entrance”): $P = 0$;

The air flow velocity spatial components on a “wall”:

$$u_1 = u_2 = u_3; \quad (14)$$

The pressure in the nasopharynx (“exit”) at an inspiration:

$$P = 50 \cdot \cos(\pi(0.87\tau + 0.5)) + 50; \quad (15)$$

The pressure in the nasopharynx (“exit”) at an expiration:

$$P = 50 \cdot \sin(\pi(1.18\tau + 0.5)) - 50; \quad (16)$$

During the simulation several significant results such as three-dimensional velocity and pressure flow field were gained. We also designed motion trajectories of small volumes of air flow. The visualization of these trajectories allowed us to reveal the different-scale turbulent swirls. The result of simulation of air flow motion trajectories inside of the maxillary sinuses is presented on the Fig. 5. Fig. 5a shows the results of air flow simulation from a patient before surgery to remove cysts. The Fig. 5b shows the results of air flow simulation from a patient after surgery to remove cysts. Removal of the cyst was carried out through an artificial anastomosis created during surgery.

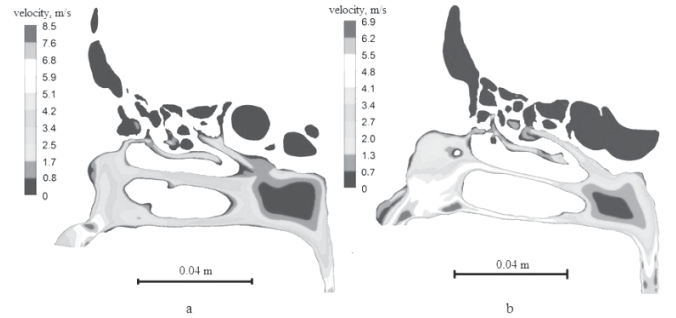


Fig. 4. Simulation of air flow in a human nasal cavities. DES-SST method. The velocity field: (a) inhalation; (b) exhalation

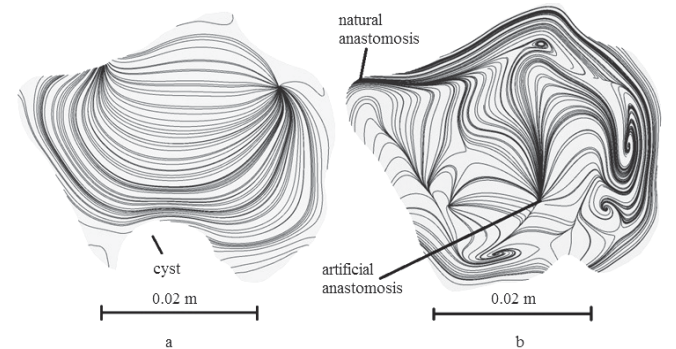


Fig. 5. Air flow motion trajectories inside of the human maxillary sinuses: (a) before surgery; (b) after surgery

Application of transient DES model to turbulent flow in area determined by the small-scale irregular mesh allowed to

capture the turbulent eddies and their spatial evolution in time. Small eddies create high-frequency oscillation components of dynamic turbulent flow parameters. DES model requires an appropriate level of computing resources. DES model was applied to simulate air flow motion trajectories in maxillary sinuses of the patient. Qualitative image of eddies structures in maxillary sinuses before (Fig. 5a) and after (Fig. 5b) a cyst excision objectively shows convective flows inside the maxillary sinuses. Thus a qualitative analysis can become one of the important diagnostic instruments.

B. Results of simulation of inhalation and exhalation at an artificial model of nose

The solid model of the nasal cavity was created on the basis of the computer tomography data (Fig. 6). The model was used for an experimental simulation of breathing process. The air motion imitation of breathing was performed through a tube, that was fixed to the nasopharynx area of the model. The piezoresistive pressure sensors was located in multiple places of the solid model for the pressure drop fixing of air flow in time.

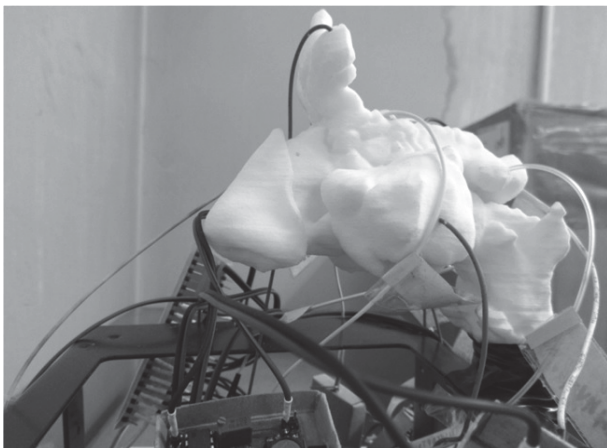


Fig. 6. Artificial solid model of human nose cavity

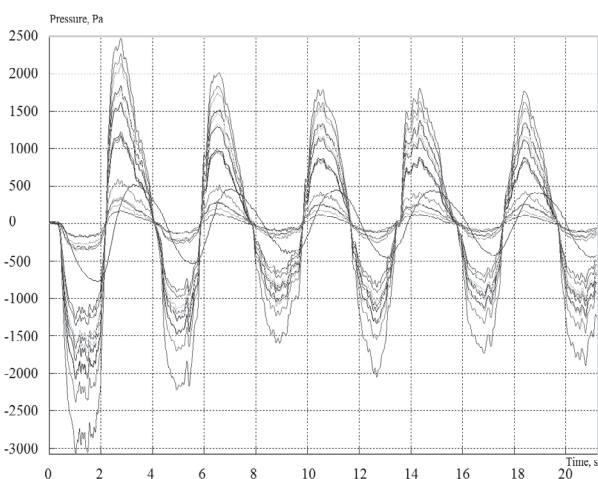


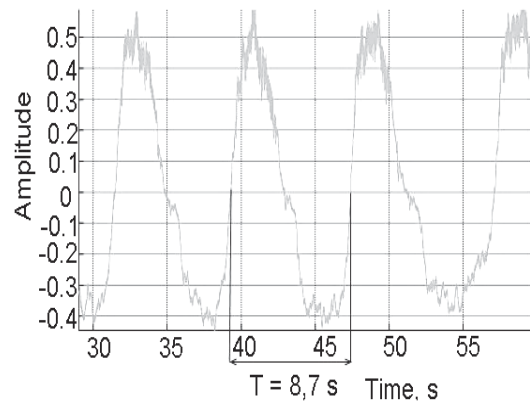
Fig. 7. Results of air flow modeling in the solid model of nose

Fig. 7 shows the results of air flow modeling in the artificial solid model of the nasal cavity. Some sinuses in the ethmoidal labyrinth were isolated from the air stream (in this case the middle cell of the right ethmoidal labyrinth) and the pressure

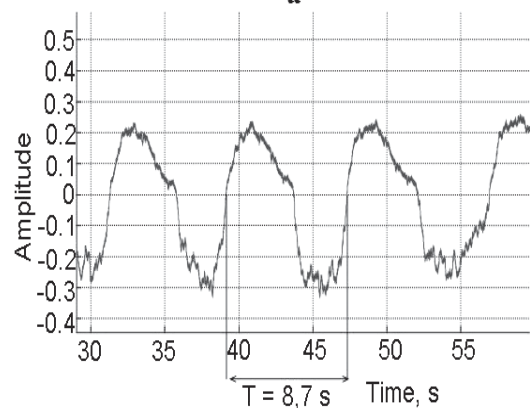
was not measured in them. This is due to the fact that it can stick together at the person.

C. Results of measuring dynamical parameters of breathing with the help of sensor devices

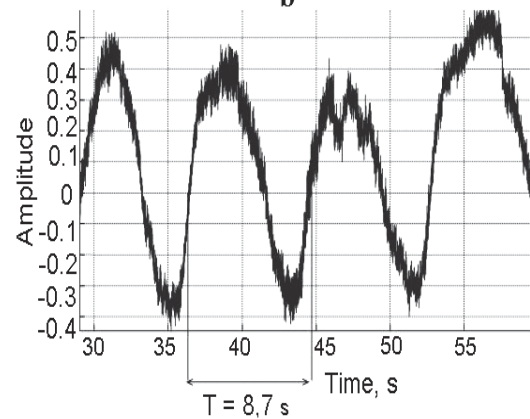
The typical results of measuring made with sensor devices are shown in the Fig.8. The results of the present study showed the dynamical character of breathing. They also show the high sensitivity of the optocouple in respect to the changes of CO₂ concentration during respiration.



a



b



c

Fig. 8. The results of the measurements of respiration fluctuations: (a) for measured pressure in the right nasal cavity; (b) for measured pressure in the left nasal cavity; (c) for IR optocouple.

D. Comparison of measurement results

Fig. 7 and 8 shows similar results. At the breath rhythm oscillations superimposed high-frequency oscillations. The spectral power density graphs of these fluctuations create additional high-frequency peaks (Fig. 9, 10). Growth in the number of peaks in the high frequency range characterizes get out of breath time, which occurs in diseases.

D. Comparison of measurement results

Fig. 7 and 8 shows similar results. At the breath rhythm oscillations superimposed high-frequency oscillations. The spectral power density graphs of these fluctuations create additional high-frequency peaks (Fig. 9, 10). Growth in the number of peaks in the high frequency range characterizes get out of breath time, which occurs in diseases.

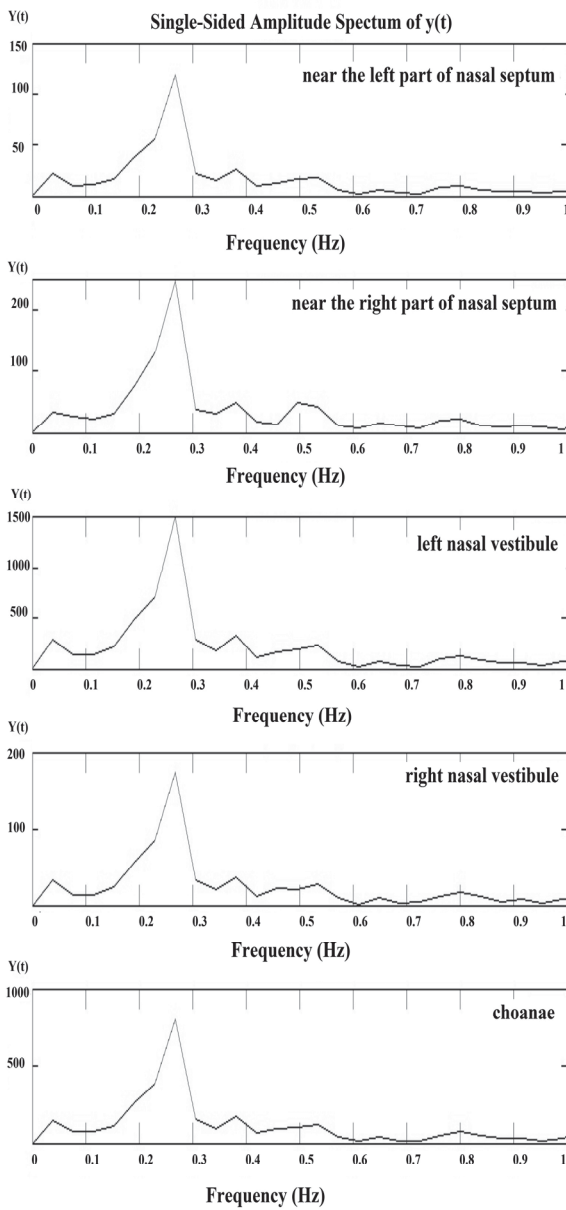


Fig. 9. The graphs of the power spectral density in the different parts of artificial solid model of nose

E. Dynamic characteristic estimation

The results of data processing as a dynamical chaotic process in packet of mathematical modeling MATLAB are shown in Fig. 11. It presents reconstructed attractor for measuring data for healthy person and for asthmatic. Growth of chaotic oscillations leads to a complication of the attractor form.

Table I shows the results of calculating of the equations (5) and (6) the correlation dimension and the correlation entropy for the group of patients with upper airways diseases.

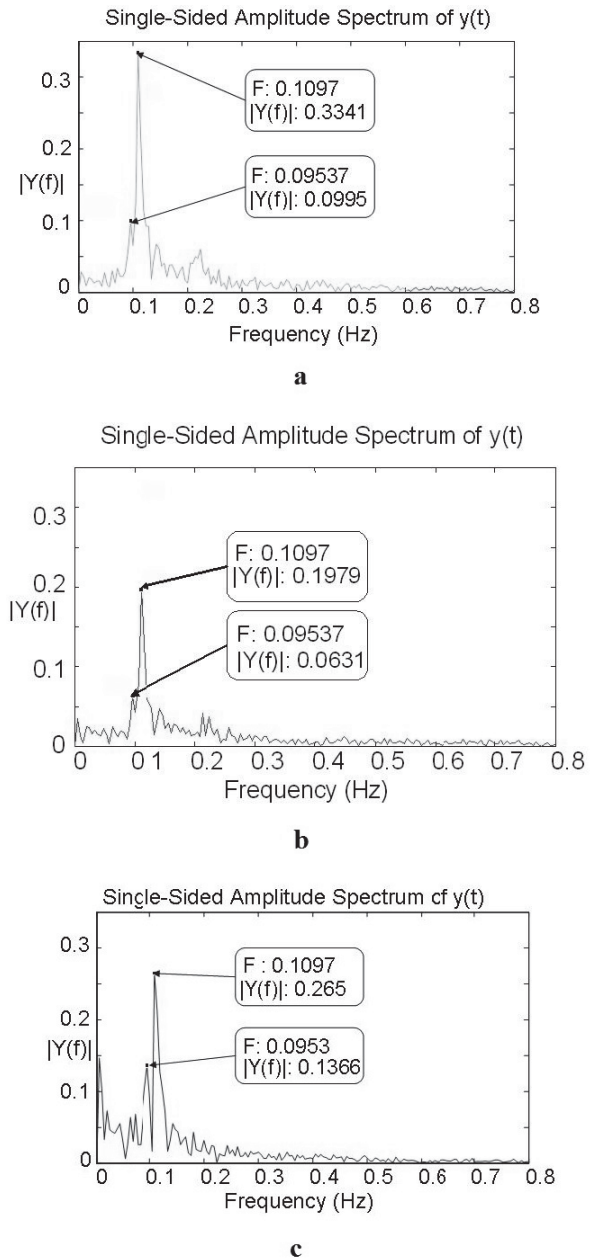


Fig. 10. The graphs of the power spectral density: (a) for measured pressure in the right nasal cavity; (b) for measured pressure in the left nasal cavity; (c) for IR optocouple.

F. Results of Raman sensor system measuring

In order to analyze human breath events an experimental setup as shown in Fig. 12 was used. With this setup it was possible to achieve inhalation and exhalation breath events with a time resolution of 250 ms. Taking into consideration a significant dependence of the Raman spectra on temperature and pressure, the setup was equipped with the pressure indicator and thermocouple of K type. In the experiments presented in this study the temperature variation was kept within $\pm 5 K$ and a pressure variation occurs only in a range of $\pm 25 hPa$ (compare with given in [23] 10 K and 1 MPa, respectively).

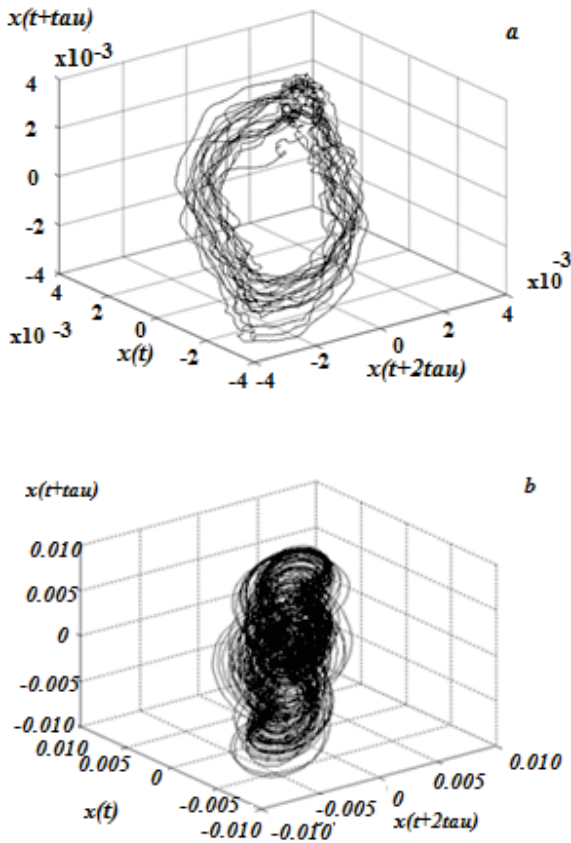


Fig. 11. Reconstructed attractor for fluctuation of velocity of air flow vortex in the vestibule of nose: a - for healthy person; b - for asthma patient

In Fig. 13a measurement series for three consecutive breath events is presented. The measurements were done with the setup shown in Fig.12. The vacuum pump in Fig.12 has an adjustable flow rate, being set to a constant value in order to ensure a sufficient sample renewal within the test cell. At starting the measurement series, the typical room air was analyzed with concentrations of the components as follows: $N_2=78.5 vol.%, O_2=20.7 vol.%, CO_2=0.1 vol.%,$ and $H_2O=0.69 vol.%. After 17 s$ a pressure drop down to 965 hPa was observed caused by starting of the inspiration cycle. The component concentration was kept constant until the expiratory gas enters the measurement cell. After 26 s since starting the measurements, the pressure is increased up to 0.995 hPa caused by starting of the expiration cycle. With a time delay of 2 seconds the expiratory gas entered into the

measurement cell and the concentration changes could be observed. Since the expiratory air has a high water vapor content ($H_2O = 3.31 vol.%$), the component concentrations was changed giving the following values: 77.92 vol.% for N_2 , 13.60 vol.% for O_2 and 5.18 vol.% for CO_2 .

All expiratory events show small concentration fluctuations. These fluctuations can be clearly resolved by the Raman sensor. In order to show that in more detail, two single shot spectra taken during the third expiratory event between 72 s and 83 s are compared in Fig. 6. The corresponding measurement moments are marked with black points and red dots in Fig. 13. These CO_2 Raman spectra are displayed in Fig. 14 and differences are clearly noticeable. The corresponding CO_2 concentrations are 4.3 vol.% and 5.12 vol.%.

TABLE I. CORRELATION DIMENSION AND CORRELATION ENTROPY

Patient	Correlation dimension		Correlation entropy	
	before treatment	after treatment	before treatment	after treatment
Patient1	2.22	2.09	0.36	0.32
Patient2	2.05	2.05	0.34	0.38
Patient3	2.19	2.10	0.38	0.35
Patient4	2.34	2.09	0.42	0.33
Patient5	2.21	2.08	0.36	0.35
Patient6	2.15	2.08	0.39	0.40
Patient7	2.18	2.08	0.39	0.33
Patient8	2.20	2.09	0.25	0.26
Patient9	2.33	2.11	0.40	0.27
Patient10	2.23	2.16	0.26	0.34

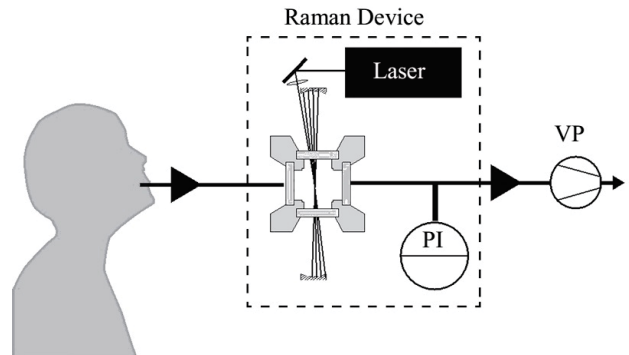


Fig. 12. Raman spectroscopy setup used for analysis of human breath events (PI – pressure indicator; TC – thermocouple; VP – vacuum pump)

However, the concentration fluctuations for N_2 (see Fig.13) quite fit in well studied dependence of the solubility of nitrogen in the blood depending on the air pressure and can manifest itself as decompression sickness.

I. CONCLUSION

Despite the large range of commercially available sensors, there is always the problem, the solution of which requires specially designed sensors. To get information on the process need to consume some of its energy. But the more energy will take the sensor from the measurement object, the stronger he misrepresented his condition. Therefore, the use of high-speed miniaturized sensors allows getting the essential information

about the process under study and better understanding its behavior under conditions of rapid change.

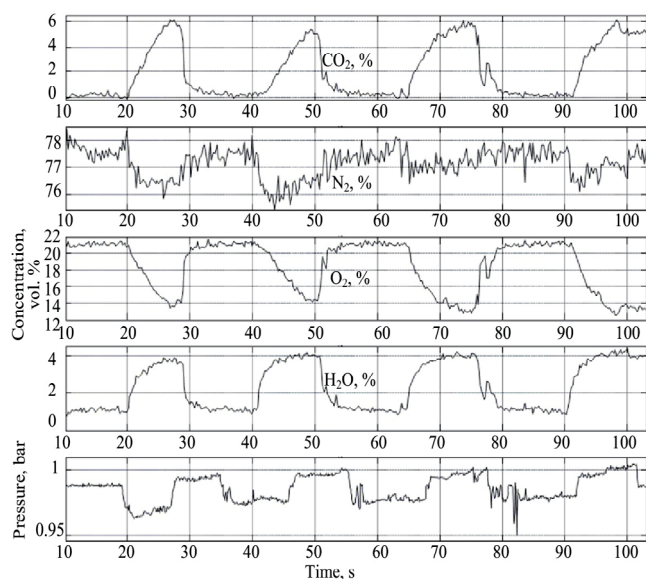


Fig. 13. Measurement series showing the component concentration and the pressure variation during three consecutive breath events. The CO_2 spectra in two indicated measurement points (they are shown between 70 s and 75 s on the CO_2 plot) are displayed below in Fig. 14

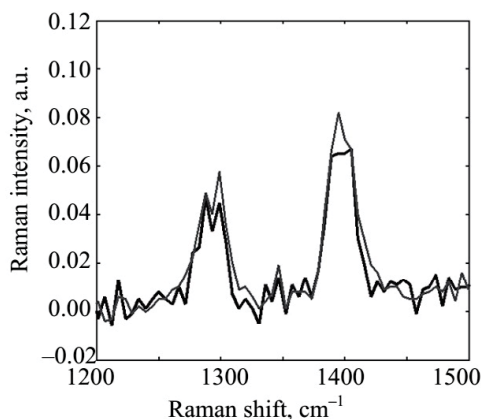


Fig. 14. The CO_2 single shot Raman spectra recorded during the measurement in the points marked in Fig. 13.

For a better understanding, it is also necessary to apply different models, refine them based on a comparison with the results of measurements. Among these models can be both numerical computer models, natural models, and dynamic models.

The presented Raman spectrum method is capable to identify and quantify all major air components of interest during a single breath event with a time resolution of 250 ms. The absolute pressure is typically between 950 and 1000 hPa. The Raman spectrum method is able to measure the gas components concentration online without any sample preparation. In order to increase the Raman signal and to enable short measurement times of 250 ms, the sensor is equipped with the near-confocal cavity. The applicability of this Raman system for analysis of the single breath events was

demonstrated. All components of interest were measured and clearly resolved online with small concentration fluctuations of 0.82 vol.% or less. The results obtained demonstrate the potential of presented Raman sensor for the future respiratory function investigations.

ACKNOWLEDGMENT

The authors are grateful to their collaborators from "LED Microsensor NT", Ltd. (N. Stoyanov, S. Kizhaev, S. Molchanov and T. Gurina) for supplying them with the LEDs and optocouples and for useful advice and assistance in carrying out this research.

REFERENCES

- [1] Stepanov E.V. "Methods of high sensitive gas analysis of molecular biomarkers in studies of exhaled air" *Trudy instituta obshchey fiziki im. A.M. Prokhorova [Proceedings of the General Physics Institute named after AM Prokhorov]*, 2005, vol. 61, pp. 1–47. [in Russian].
- [2] Spalart P.R., Jou W.-H., Strelets M., Allmaras S.R. "Comments on the feasibility of LES for wings, and on a hybrid RANS/LES approach" in *Proc. of First AFOSR International Conference on DNS/LES*. Ruston, Louisiana: Greyden Press, 1997. pp. 137–147.
- [3] Travin A., Shur M., Strelets M., Spalart P. "Detached-Eddy Simulations Past a Circular Cylinder" *Flow, Turbulence and Combustion*. 1999, vol. 63, N 1–4, pp. 293–313.
- [4] Travin A., Shur M., Strelets M., Spalart P.R. "Physical and numerical upgrades in the detached-eddy simulation of complex turbulent flows" *412 Euromech Colloquium on LES of complex transitional and turbulent flows*. Abstracts. Munich, Germany, 2000, pp. 87–93.
- [5] Menter F.R. Zonal "Two Equation $k - \omega$ Turbulence Models for Aerodynamic Flows" *AIAA Paper*, 1993, vol. 93-2906, 21 p.
- [6] Spalart P.R., Deck S., Shur M.L., Squires K.D., Strelets M.Kh., Travin A. "A new version of detached-eddy simulation, resistant to ambiguous grid densities" *Theoretical and Computational Fluid Dynamics*, 2006, vol. 20, N 3, pp. 181–195.
- [7] Shur M.L., Spalart P.R., Strelets M.Kh., Travin A.K. "A hybrid RANS-LES approach with delayed-DES and wall-modelled LES capabilities" *International Journal of Heat and Fluid Flow*, 2008, vol. 29, N 6, pp. 1638–1649.
- [8] Sagalovich B. M. *Physiology and pathophysiology of the respiratory passages*. M.: Medicine, 1964, 394 pp. [in Russian].
- [9] Mlynski G., Grützenmacher S., Plontke S., Mlynski Barbara, Lang C. "Correlation of nasal morphology and respiratory function" *Rhinology*, 2001, vol. 39, pp. 197–201.
- [10] Lukyanov G., Rassadina A., Usachev V. "Comparison and the analysis of the processes of the movement of air through the human breathing system and its natural model" in *Proceedings International Conference on Physics and Control. PhysCon 2005*, pp. 872-875.
- [11] Voronin A.A., Lukyanov G.N., Frolov E.V. "Detached-eddy simulation of turbulent airflow" *Scientific and Technical Journal of Information Technologies, Mechanics and Optics*, 2014, N 1 (89), pp. 187-192. [in Russian].
- [12] Lukjanov G.N., Rassadina A.A., Dranishnikova O.A., Skirmandt E.V., Usachev V.F. "Research of Warm and Mass Exchanged Characteristics of Breathing" *Journal of Instrument Engineering*, 2005, vol. 48, N 5, pp. 63-66. [in Russian].
- [13] Yanov, Y., Shcherbakova N., Nacharov P. "An analysis of the gas composition of exhaled air in the diagnosis of diseases" *Russian Otorhinolaryngology*, 2005, N 4, pp. 126–132. [in Russian].
- [14] Herbig J., Müller M., Schallhart S., Titzmann T., Graus M., Hansel A. "On-line breath analysis with PTR-TOF" *Journal of Breath Research*, 2009, vol. 3, N 2, art. 027004. doi: 10.1088/1752-7155/3/2/027004
- [15] Schulze-König T., Wacker L., Synal H.-A. "Direct radiocarbon analysis of exhaled air" *Journal of Analytical Atomic Spectrometry*, 2011, vol. 26, N 2, pp. 287–292. doi: 10.1039/C0JA00039F

- [16] Portner P.M., LaForge D.H. "Method and Apparatus for Pulmonary Function Analysis". Patent US4083367, 1978.
- [17] Schlüter S., Popovska-Leipertz N., Seeger T., Leipertz A. "Gas sensor for volatile anesthetic agents based on Raman scattering" *Physics Procedia*, 2012, vol. 39, pp. 835–842. doi: 10.1016/j.phpro.2012.10.108
- [18] Schlüter S., Asbach S., Popovska-Leipertz N., Seeger T., Leipertz A. "A signal enhanced portable Raman probe for anesthetic gas monitoring" *Scientific and Technical Journal of Information Technologies, Mechanics and Optics*, 2015, vol. 15, N 2, pp. 215–226. doi: 10.17586/2226-1494-2015-15-2-218-226
- [19] Schrader B., Bougeard D. *Infrared and Raman Spectroscopy. Methods and Applications*. NY: Wiley-VCH, Weinheim, 1995, 787 p.
- [20] Tobin M. C. *Laser Raman Spectroscopy*. NY: Wiley-Interscience, 1971, 171 p.
- [21] Herzberg G. *Molecular Spectra and Molecular Structure. I. Spectra of diatomic molecules*. 2nd ed. D. van Nostrand Company Inc., 1966. 672 p.
- [22] Herzberg G. *Molecular Spectra and Molecular Structure. II. Infrared and Raman spectra of polyatomic molecules*. 2nd ed. D. van Nostrand Company Inc., 1966, 644 p. Eichmann S.C., Weschta M., Kiefer J., Seeger T., Leipertz A. "Characterization of a fast gas analyzer based on Raman scattering for the analysis of synthesis gas" *Review of Scientific Instruments*, 2010, vol. 81, N 12, Art. 125104. doi: 10.1063/1.3521397